TiO_2 Nanorods as Electron Transport Layer for Inorganic Perovskite Solar Cells

M.Tech. Thesis

By

HARSH VAID

DISCIPLINE OF METALLURGY ENGINEERING AND MATERIALS SCIENCE

INDIAN INSTITUTE OF TECHNOLOGY INDORE

JUNE 2019

TiO_2 Nanorods as Electron Transport Layer for Inorganic Perovskite Solar Cells

A THESIS

Submitted in partial fulfilment of the
requirements for the award of the degree
of
Master of Technology

by

HARSH VAID

DISCIPLINE OF METALLURGY ENGINEERING AND MATERIALS SCIENCE
INDIAN INSTITUTE OF TECHNOLOGY INDORE
JUNE 2019

INDIAN INSTITUTE OF TECHNOLOGY INDORE

CANDIDATE's DECLERATION

I hereby certify that the work which is being presented in the thesis entitled " **TiO_2 Nanorods as Electron Transport Layer for Inorganic Perovskite Solar Cells**" in the partial fulfilment of the requirements for the award of the degree of **Master of Technology** and submitted in the discipline of **Metallurgy Engineering and Materials Science, Indian Institute of Technology Indore,** is an authentic record of my own work carried out during the time period from July 2017 to June 2019 under the supervision of Dr. Ajay Kumar Kushwaha and Dr. Mrigendra Dubey at IIT Indore. The matter presented in this thesis has not been submitted by me for the award of any other degree of this or any other institute.

Signature of the student with date

(HARSH VAID)

This is to certify that the above statement made by the candidate is correct to the best of my/own knowledge.

Signature of the supervisor of M.Tech thesis (with date)

(Dr. Ajay Kumar Kushwaha)

Signature of the supervisor of M.Tech thesis (with date)

(Dr. Mrigendra Dubey)

Signature of Supervisor of M. Tech Thesis

Date:

Convener, DPGC

Date:

Signature of PSPC Member #1

Date:

Signature of PSPC Member #2

Date:

ACKNOWLEDGEMENTS

I would like to express my sincere thanks of gratitude to my guide Dr. Ajay Kumar Kushwaha for providing me this great opportunity to work under him. His timely advice, untiring guidance, and scientific approach have helped me in accomplishing my work. Without his constant inspiration and encouragement, it would not have been possible for me to complete this research work. I would like to acknowledge Head, MEMS discipline for providing several research facilities and infrastructure. I also thank my co-supervisor Dr. Mrigendra Dubey for supporting and monitoring me during my project. I would also like to thank the members of my PSPC committee, Dr. Hem Chandra Jha and Dr. Sunil Kumar for their constant support and vital suggestions throughout this work. The insights provided by them helped me to understand theoretical as well as practical aspects of this work. I am grateful for FESEM and XRD facilities provided at the Sophisticated Instrument Centre (SIC), IIT Indore. I am very happy to attribute my thank to SERB, Government of India, for support of consumables and other equipment's under ECRA project. I also thank my lab mates Mr. Mukurala Nagaraju, Mr. Aditya Bhardwaj and Hariom Sharma for their continuous support and valuable suggestions. I would like to acknowledge my family for their affection, care and untiring support. Finally, I would like to express my sincere gratitude to the Almighty.

- Harsh Vaid

Dedicated to

“My Parents and My Loving Sister”

Abstract

Electron transport layer plays an important role in facilitating the flow of negative charge carriers in Perovskite Solar cells. In the field of Inorganic Perovskites, we have specifically optimised TiO_2 as Electron Transport material. TiO_2 Nanorods were synthesised by hydrothermal synthesis at different precursor concentration and reaction times. The most optimised result was obtained at 0.7 ml concentration of Titanium butoxide and reaction time of 4 hours. XRD analysis confirmed the structural formation of Rutile TiO_2 nanostructures, Optical behaviour were studied by UV-Visible spectroscopy and the bandgap of 2.3 eV in TiO_2 nanostructures was obtained. The surface morphology was observed by FESEM, that showed the formation of TiO_2 Nanorods. Cyclic Voltammetry and chronoamperometry were performed to evaluate the photocurrent response and long-term photo stability of the thin film. Open circuit potentiometry was done to evaluate the career life time of charge carriers in the TiO_2 thin films.

Inorganic perovskite $CsPbBr_3$ was prepared by spin coating method and its structure was confirmed by XRD spectroscopy. UV Visible spectroscopy provided the absorption spectra which determined the band gap (2.3 eV) of our perovskite material. The SEM images confirmed the formation of the perovskite cubic structure. Finally, we tried to synthesise the all inorganic perovskite solar cell FTO/TiO_2/$CsPbBr_3$/NiO/Ag. The dark current profile of the devise shows similar response as that of a p-n junction diode. But the device failed to show any photo response in presence of light.

CONTENTS

Chapter 3: EXPERIMENTAL AND CHARACTERIZATION TECHNIQUES

List of Figures

List of Abbreviations

S.No.	Abbreviation	Meaning
1	ETL	Electron Transport Layer
2	PVK	Perovskite
3	PSC	Perovskite Solar Cell
4	PCE	Power Conversion Efficiency
5	FTO	Fluorine doped Tin Oxide
6	HTL	Hole Transport Layer
7	EHP	Electron Hole Pair
8	NR’s	Nanorods

List of Symbols

S.No.	Symbol	Meaning
1.	Σ	Conductivity
2.	λ	X-ray wavelength
3.	L	Length
4.	C	Concentration
5.	ε	Absorption co-efficient
6.	T	Transmittance
7.	t	Thickness
8.	A	Absorbance
9.	D	Crystallite size
10.	E_g	Band gap
11.	β	Full width half maxima (FWHM)
12.	Θ	Bragg's angle
13.	I	Intensity of transmitted light
14.	I_o	Intensity of incident light
15.	I_{pc}	Photocurrent
16.	I_{sc}	Short circuit current
17.	V_{oc}	Open-circuit voltage
18.	L_e	Diffusion length of electron
19.	L_h	Diffusion length of hole
20.	K_b	Boltzmann Constant

CHAPTER 1

INTRODUCTION

1.1 Solar Cell

Solar cell or photovoltaic cell can be defined as ‘‘an electrical device that converts the light energy directly into electrical energy’’. When photons or light strikes on the surface of solar cell, the energy is absorbed by the electrons present in valance band and if the energy is more than the energy band gap of the absorber material then electrons get excited from valance band to conduction band, that results in formation of exciton i.e. electron-hole pair [**1**]. After separation of charge careers of opposite nature, they are supplied to the external circuit. Till date, many solar cell technologies have been introduced like silicon solar cells (monocrystalline, polycrystalline, and amorphous), dye- sensitised solar cells, perovskite solar cells etc. Silicon based solar cells are commercially used in industries and households while the DSSC and perovskite solar cells are still under research and development.

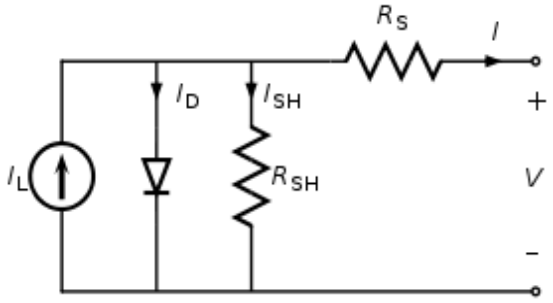

Fig. 1 Electrical equivalent circuit of solar cell [2]

The figure shows electrical equivalent of a practical solar cell device as it also consists of series and shunt resistors. In an ideal solar cell circuit, no losses are considered, and the equivalent circuit simply consists of a diode with a current source in parallel.

The current developed by the solar cell is given as:

$$I = I_l - I_d - I_{sh}$$

1.2 Generations of Solar Cells:

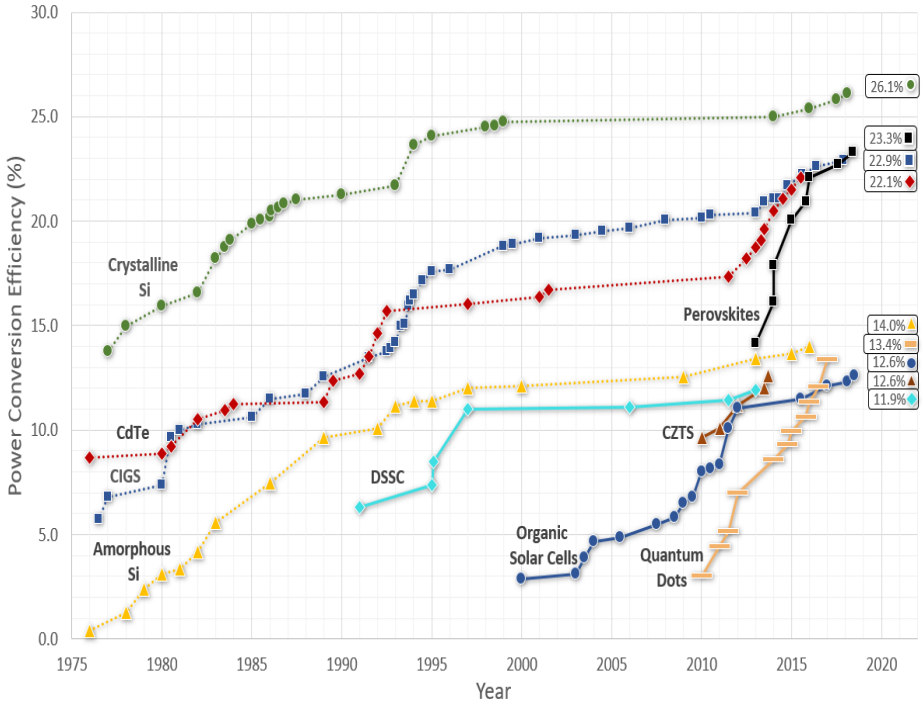

Fig. 2 Growth of different generation solar cells [3]

1st Generation Solar Cells

Silicon was used to process most of the traditional solar cell devices. These are ambiently stable as well as most efficient solar cells that exists for residential and commercial use and account for more than 80% of the solar panels sold around the world **[4]**. Currently there are three type of silicon solar cell technologies available:

(a) **Monocrystalline Silicon Solar Panels:** This is the oldest solar cell technology and still being the most prevalent and efficient in this field. These solar panels work even in low light conditions and have recorded a maximum efficiency of around 24%. Although, these are most expensive panels in the market, therefore their alternatives are being explored to obtain similar performance at lower costs.

(b) **Polycrystalline Silicon Solar Panels:** These are made from multiple silicon crystals instead of pure silicon single crystal. They are less expensive because the processing conditions are not to be monitored carefully but they have less power conversion efficiency (up to 19.3 %) when compared from monocrystalline silicon solar cells. **[5]**

(c) **Amorphous Silicon Solar Panels:** Despite growing silicon crystals, here silicon is deposited on thin layer substrate. The production processes involve less energy consumption than crystalline panels and open the gates for flexible solar cell technology. The disadvantage of these panels is their less power conversion efficiencies up to 10 %. **[5]**

2nd Generation Solar Cells

When compared from crystalline silicon solar cells, these are termed as thin film solar cells because semiconducting materials with a thickness of few micrometres are used to process them. There are three categories of solar cells that comes under this group. They are amorphous silicon, copper indium gallium selenide (CIGS) and cadmium telluride (CdTe). [**6**].

3rd Generation Solar Cells

The new generation of solar cells is focussed on new materials besides silicon. The target is to obtain high power conversion efficiencies, highly stable devices at ambient conditions, and making the energy conversion less

expensive. In this field, perovskite (ABX_3) are very promising materials for light to electrical energy conversion.

1.3 Introduction to Perovskite Solar Cells

Perovskite solar cell is a type of solar cell having perovskite material present in its active layer for light absorption. Perovskite is a calcium titanium oxide mineral composed of calcium titanite ($CaTiO_3$) **[7]**. The name is also applied for the entire class of compounds having similar crystal structure. Perovskite solar cells based on organic/inorganic metal halide (ABX_3) absorbers have proved to be very promising in photovoltaic technology because of their superb power conversion efficiencies along with low materials cost. Based on materials, perovskite solar cells can be broadly classified as organic-inorganic perovskite solar cells and all inorganic perovskite solar cells

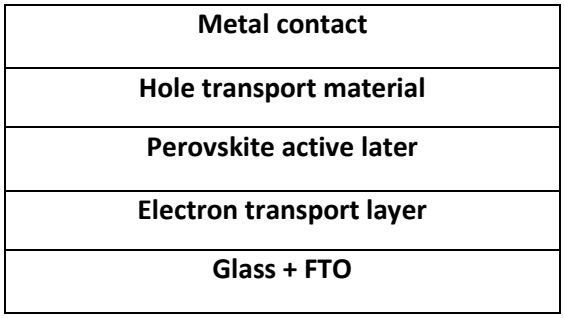

Fig. 3 Layered structure of perovskite solar cell

1.4 Based on Materials Classification Perovskite Solar Cells can be broadly classified as:

(a) Organic-Inorganic Hybrid Perovskite Solar Cells:

Organic-inorganic hybrid perovskite solar cells have attracted keen attention because of the rapid growth in power conversion efficiencies that

they have attained since 2009 **[8]**. The highest reported power conversion efficiency of solar cell device based on this material is more than 22%, which is almost equal to that of conventional monocrystalline silicon solar cells. This exceptional performance is due to the hybrid perovskite material i.e. ABX_3, where A is CH_3NH_3, B is a divalent metal (Sn or Pb), and X is the non-metal halide (Cl, Br, I). the material shows excellent optoelectronic properties that results in the outstanding performance of the solar cell device. Although, organic-inorganic hybrid perovskite solar cells have attained such high PCE's, they suffer from poor stability in ambient conditions and degrades in small amount of time. Hence, there real time application is restricted. Replacement of organic compound i.e. CH_3NH_3 by the inorganic cations like Ca, Rb, K etc can be a solution to improve the stability of the perovskite crystal structure.

(b) All Inorganic Perovskite Solar Cells:

Inorganic perovskite lists a lot of materials including $CsSnI_3$, $CsPbI_3$, and CsPbBr3 etc. Lead based inorganic perovskite have proved them to be more efficient and have reported the highest power conversion efficiencies of 13.21 % **[9]**, whereas Sn based perovskite have achieved the power conversion efficiencies of around 3 %. They show improved stability in ambient conditions as compared to their organic counterparts. Like any other perovskite solar cell, the structure of Inorganic perovskite solar cell consists of three different operational layers in which the first layer is electron transport layer which is deposited over the FTO substrate, followed by the active perovskite absorber layer in which the absorption of sunlight occurs that results in the formation of electron-hole pairs. The third layer is the hole transport layer which facilitates the flow of positive charge carriers i.e. holes towards the device contacts. We will majorly focus on lead based all inorganic perovskite solar cells because they have better probability for their practical implementation in real world, because of the better stability

that they show in ambient conditions when compared to the organic inorganic hybrid perovskite solar cells.

1.5 Working Mechanism of Perovskite Solar Cell:

When photons of light energy fall over the active layer of the perovskite solar cell FTO/TiO_2/$CsPbBr_3$/HTM/Au, it results in the generation of electron-hole pair, when the excitation energy is more than the bandgap of the perovskite material. The charge careers generated have the tendency to move towards lower energy state present within that material. Hence, the electrons get transported from higher energy perovskite active layer towards lower energy electron transport material, whereas the holes flow from lower to higher energy level i.e. from perovskite to hole transport layer. The electrons then move from the ETL to the FTO contact while the holes on the other side are transmitted towards the gold contacts via hole transport material.

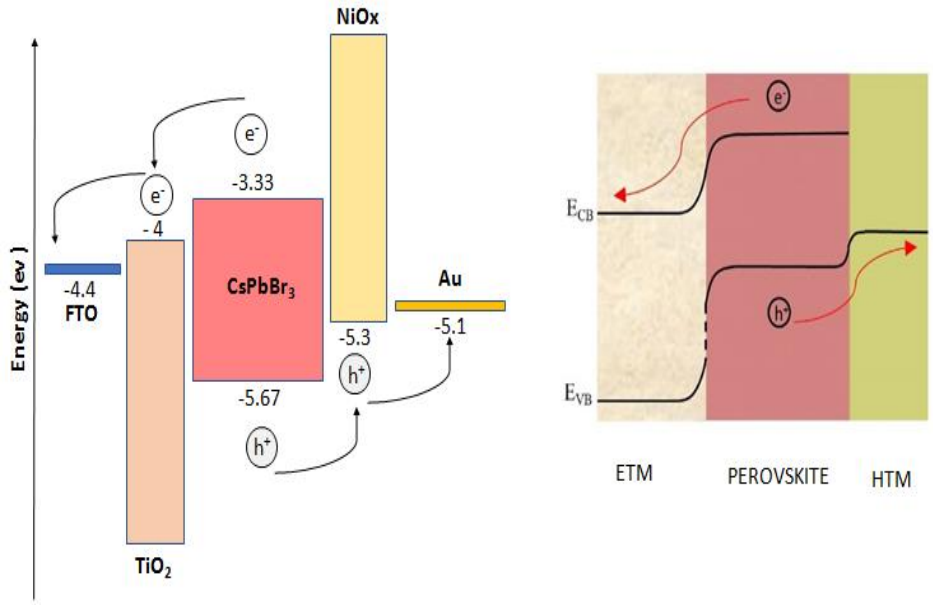

Fig. 4 Working principle of perovskite solar cell

1.6 Efficiency and Stability of Perovskite Solar Cells

Organic inorganic hybrid perovskite solar cells have achieved power conversion efficiencies of over 22 % [**10**]. Such high PCE's have been achieved by low cost solution processed techniques. Their practical implementation is still restricted due to less material stability because of the presence of the organic material. Replacing organic–inorganic hybrid perovskite material with inorganic perovskite is a promising solution in increasing the stability of the cell. The inorganic perovskite based solar cells lacks in higher efficiencies as obtained in organic-inorganic hybrid perovskite solar cells.

1.7 Advantages of Perovskite Solar Cells Over Silicon Solar Cells:

- Perovskite have high absorption capabilities as compared to silicon. Merely 1cm thick perovskite film can absorb 10^4 photons /cm^2 [**11**], while a minimum of 3 cm thick silicon sheet is required for absorbance phenomenon, otherwise no absorbance of photons will take place and the device based on it will not work as solar cell.
- Perovskite open the gates for the flexible solar cell technology, as very thin films can be synthesised for fabricating solar cell devices.
- Perovskite materials have direct band gap as compared to indirect band gap in silicon.
- Synthesis of perovskite solar cells involves low cost, easy fabrication and comparable PCEs as that of silicon solar cells.

1.8 Existing Issues in Perovskite based Solar Cells

Organic inorganic hybrid perovskite solar cells are facing the stability related problems due to the presence of organic compound. In case of inorganic perovskites, the stability of the structure is improved but the reduction of power conversion efficiency is a major issue. Lead based

inorganic perovskite shows better results in terms of power conversion efficiencies but as lead is hazardous material people are trying to develop lead free inorganic perovskites and to get better results.

1.9 Organization of the Thesis

Chapter 1 describes the basics of solar cell devices and its various generations. It also includes discussion about the stability and efficiency related issues in Perovskite solar cell devices.

Chapter 2 provides an insight to the layered structure of perovskite solar cell and explains how it works by means of its electronic diagram. It includes discussion about different types of ETL's and majorly targets on TiO_2 based ETL. It also discusses about active perovskite material and about different HTM's.

Chapter 3 discusses about the experimental techniques used for synthesis of TiO_2 nanorods i.e. hydrothermal method and $CsPbBr_3$ nanoparticles by solution processing method. It also includes the detailed discussion about various characterization techniques like XRD, UV Visible spectroscopy, FESEM and Electrochemical set up for photocurrent measurements.

Chapter 4 deals with the results and discussions of the experimental work done under this project. It demonstrates the optimized growth parameters for the growth of TiO_2 nanostructures for its application in perovskite solar cells. It also shows the structural, optical and morphological properties of $CsPbBr_3$ nanoparticles.

Chapter 5 concludes the work described in the thesis and discusses about the future scope of this work.

CHAPTER 2

LITERATURE SURVEY

2.1 All Inorganic Perovskite Solar Cell:

The term all inorganic perovskite solar cell corresponds to inorganic ETM, inorganic perovskite and inorganic HTM materials. As discussed, stability is the major concern for organic materials at ambient conditions, the device should be made up of such materials that can remain stable at room temperature and pressure. Hence, if all the layers of a solar cell are made of inorganic materials then it will result in more stable device. Inorganic perovskite lists a lot of materials including $CsSnI_3$, $CsPbI_3$, and CsPbBr3 etc. For the purpose of ETL TiO_2 is a good choice. HTM can be synthesised from NiO nanoparticles. Lead based inorganic perovskite have proved them to be more efficient and have reported the highest power conversion efficiencies of 13.21 %, whereas Sn based perovskite have achieved the power conversion efficiencies of around 3 %.

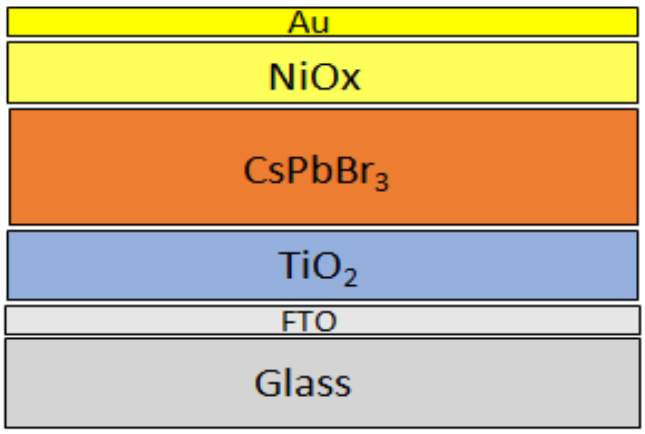

Fig. 5 Layered structure of inorganic perovskite solar cell

The layered structure of Inorganic perovskite solar cell consists of three different operational layers. The first layer is the electron transport layer which is deposited over the FTO substrate, the second layer is the perovskite

absorber layer in which the absorption of sunlight occurs that results in the formation of electron hole pairs, the third layer is the hole transport layer which facilitates the flow of positive charge carriers i.e. holes towards the device contacts.

In inorganic perovskite solar cell, the sunlight falls over the $CsPbBr_3$ absorber layer through Glass/FTO/TiO_2 layers of the device. Electron transport layer is synthesised in a way to get maximum transparency so that most of the light passes through it and strikes on the perovskite absorber layer so that maximum number of electron-hole pairs are generated.

2.2 Electron Transport Layer (ETL):

Electron Transport material or ETM between the perovskite layer and the transparent electrode (FTO/ITO) is necessary for the purpose of effective electron transport and hole blocking. Nanostructured Electron transport material offers more perovskite infiltration as compared to mesoporous electron transport material and improves electron transportation that in turn enhances the performance of perovskite solar cell. Nanostructured electron transport material can be prepared using different techniques that includes solvo-thermal method, chemical vapour deposition, electro spinning, template assisted method, sol-gel technique, hydrothermal synthesis etc. Solvo-thermal and hydro thermal synthesis methods prevent the high temperature sintering of conventional compact electron transport materials like TiO_2/ZnO nanostructures.

2.2.1 Characteristics of Electron Transport Layer:

Electron transport layer or ETL should satisfy the band alignment with perovskite layer so as the effectively collect the electrons generated in the perovskite active layer **[12]**. Technically, the conduction band of the ETL must have lower electronic energy level as compared to the conduction band of the active perovskite layer. Secondly, is should have higher transparency in the visible region of the spectrum so that maximum photons can pass

through it and produce large number of electron-hole pairs in the perovskite layer. The electron transport layer should also facilitate the smooth passage to electrons so that they can have large diffusion lengths and less rate of recombination.

2.2.2 Different Types of Electron Transport Layers:

Electron transport layer can be formed using organic or inorganic materials. The organic materials such as PEHT, PCMB etc can be used to facilitate the purpose of ETL in perovskite solar cells. But as these materials do not have much stability in ambient conditions, their inorganic counterparts are used.

Inorganic electron transport materials include TiO_2, ZnO, SnO_2, SiO_2, ZrO_2 etc. To date, TiO_2 based ETL's are most widely used by different research groups because of its advantages of providing higher power conversion efficiencies in PVK's.

2.2.3 Development of TiO_2 Nanorods Based Electron Transport Layer:

Amongst different materials that can be used for the synthesis of electron transport material, TiO_2 proves it to be a promising material as electron transport material for perovskite solar cell application. It shows wide band gap of 3.2 eV [**13**], high chemical stability, optical transparency in visible region, semiconducting properties, photo catalytic activities, high PEC efficiency, long term photo stability, low cost synthesis and nontoxic in nature. Because of all these properties, TiO_2 behaves as excellent multi-functional material in various applications including solar cell applications. Aiming TiO_2 nanostructures as ETM, Qiu et al. synthesised TiO_2 nanowire array as ETM and a perovskite solar cell having power conversion efficiency of 4.78 % in early 2013. The morphology of nanowires was studied, and it was suggested that less diameter and dense TiO_2 nanowires are favourable for high performance devices. TiO_2 nanotubes were also

synthesised on Ti foils and it even higher efficiency solar cells could be formed using these nanostructures. However, TiO_2 nanotube arrays require high temperature annealing to enable effective electron transport which makes it an expensive process [**14**]. Furthermore, TiO_2 nanorods are considered as promising electron transport material, because of its excellent electron transport capabilities in perovskite solar cells. Kim et al. proposed the employment of TiO_2 nanorods in perovskite solar cells and found that uniformly ordered and short TiO_2 nanorods are desirable for ETM in perovskite solar cell. They reported a PCE of 10% using TiO_2 nanorods as electron transport material in the device fabrication**. [15]** TiO_2 nanostructures can exist in three different crystal structures: two tetragonal forms (rutile and Anatase) and one rhombic form (brookite) [**16**]. In particular, due to their high specific surface area, TiO_2 nanostructures shows high performance levels for many applications as compared to their bulk form.

2.3 Perovskite ABX_3 for Active Layer in Perovskite Solar Cell:

ABX_3 is the general formula of perovskite material, where A and B are metals of different size and valences, while X is the halide anion which is bonded to both the metal cations.

The metal cation A occupies the corner position in the unit cell, cation B holds the body centre position and the halide X lies at face centres of the unit cell.

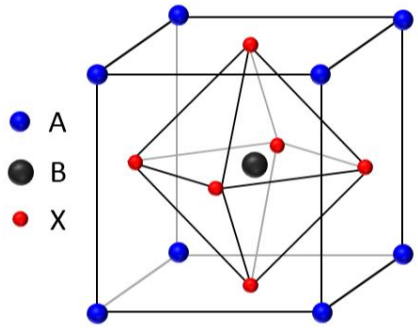

Fig. 6 Perovskite crystal structure [17]

2.3.1 Development of $CsPbBr_3$ as Active Perovskite Layer:

Synthesis of active perovskite layer by means of perovskite thin film can be done by different methods like hot injection method, solution processing method, sol-gel method, synthetic method for water stable perovskite etc. In our project work, we synthesised the perovskite thin film by solution processing method. In this. Caesium Bromide and Lead Iodide were dissolved in anhydrous DMSO solution with 1:1.2 as the concentration ratios. The obtained solution was mixed properly on magnetic stirrer for 12 hours, followed by ultrasonication for 30 minutes. The solution was coated on the FTO substrate by spin coating method and annealed at 180^{o}C for 15 minutes.

2.4 Hole Transport Layer

Hole transport layer plays a significant role in the collection of positively charged careers developed in the perovskite active layer. The HTM provides high mobility path for the holes to travel and also acts as blocking layer for the electrons. There are several materials that can be used for the purpose of HTM in perovskite solar cell application. These materials include organic as well as inorganic compounds. Spiro-OMeTAD is most popular organic HTM, while inorganic HTM include CuI, CuO, NiO, MoO_3, CuSCN etc. though, highest power conversion efficiency is observed in Spiro-OMeTAD, but it has its own limitations that include high cost and poor stability. The inorganic HTM's are good replacement of it and is used to get better stability and low-cost synthesis.

2.5 Research Challenges:

Power conversion efficiency in case of inorganic perovskite solar cells is a major challenge that researchers are facing. As of now, the highest efficiency of 13.21 % is reported in case of lead based inorganic perovskites.

Although, the stability of inorganic perovskite is more as compared to their organic counterparts, but still a lot of improvement is still required.

CHAPTER 3

EXPERIMENTAL AND CHARACTERIZATION TECHNIQUES

3.1 Experimental Techniques:

3.1.1 Synthesis of TiO_2 Nanostructures by Hydrothermal Method [18]:

TiO_2 Nanorods are synthesised using facile hydrothermal method as it is simple and economical method to synthesise well aligned nanostructures. Also using this technique, we can obtain single crystalline nanostructure of material having high specific surface areas. This method also provides better opportunity for controlling the size and morphology of the Nanorods for better photo conversion efficiencies. Hydrothermal technique involves the reaction at controlled temperatures and pressures as the reaction takes place in Teflon liner which is kept inside an autoclave for maintaining the desired conditions.

(a) Synthesis of TiO_2 NR's with change in reaction time:

Step 1:

The FTO (fluorine doped tin oxide) substrate is cleaned in different solutions including soap water (removes hydrophilic impurities), DI water (removes hydrophobic impurities), acetone, followed by ethanol or IPA solution. In Each solution, the FTO substrate is ultra-sonicated for 15 minutes.

Note: cleaning is the most important step in entire process because if substrate is not cleaned properly, the growth of nanostructure is directly affected.

Step 2:

20 ml of hydrochloric acid and DI water are mixed thoroughly by magnetic stirring for 10 minutes at 500 rpm (without heating). After proper mixing, 0.7 ml of Titanium butoxide is added to it and the new solution formed is again kept under magnetic stirring for 30 minutes. The solution is then transferred to Teflon liner in which the reaction is going to take place

Step 3:

Cleaned FTO substrate is wrapped by Teflon tape at its one end and is kept inside the Teflon liner with its conductive side facing downwards, for the controlled growth of TiO_2 nanostructures.

Step 4:

The Teflon liner is placed inside the autoclave and it is kept inside the hot oven at 160°C for different reaction times, to study to behaviour of the TiO_2 Nanorods with variation in time.

(b) Synthesis of TiO_2 NR's with change in precursor concentration:

Step 1:

The FTO (fluorine doped tin oxide) substrate is cleaned in different solutions including soap water (removes hydrophilic impurities), DI water (removes hydrophobic impurities), acetone, followed by ethanol or IPA solution. In Each solution, the FTO substrate is ultra-sonicated for 15 minutes.

Note: cleaning is the most important step in entire process because if substrate is not cleaned properly, the growth of nanostructure is directly affected.

Step 2:

20 ml of hydrochloric acid and DI water are mixed thoroughly by magnetic stirring for 10 minutes at 500 rpm (without heating). After proper mixing, different precursor concentrations 0.4ml, 0.5ml, 0.6ml and 0.7ml of Titanium butoxide is added to it and stirred for 30 minutes.

Step 3:

Cleaned FTO substrate is wrapped by Teflon tape at its one end and is kept inside the Teflon liner with its conductive side facing downwards, for the controlled growth of TiO_2 nanostructures.

Step 4:

The Teflon liner is placed inside the autoclave and it is kept inside the hot oven at 160°C for 4 hr to study to behaviour of the TiO_2 Nanorods with variation in precursor concentration.

3.1.2 Synthesis of Perovskite Nanoparticles [19]:

Step 1: A 0.45 M equimolar solution (slightly below the 0.5 M solubility limit) of perovskite precursors i.e. Caesium bromide and lead bromide in DMSO was prepared in ambient conditions, under continuous magnetic stirring at 60°C for 24 hours.

Step 2:

After continuous stirring for 24 hours, the solution was again ultra-sonicated for 30 minutes to disperse the remaining particles present in it.

Step 3:

The obtained solution is now spin coated on the cleaned glass/ FTO substrate at spinning speed of 2000 rpm for 30 seconds. The prepared thin

film is now annealed at 250°C in nitrogen filled environment to avoid oxidation of the perovskite film at higher temperatures.

3.1.3 Fabrication of Solar Cell Device and its Characterization:

The fabrication of solar cell includes the development of electron transport layer, perovskite active layer and hole transport material. The synthesis process is a sequential approach in which the ETM is developed over the FTO substrate and over it the perovskite layer is coated. The Hole transport layer is deposited on the perovskite active layer and the metal contacts are made on it. The device architecture can be abbreviated as FTO/TiO_2/$CsPbBr_3$/NiO/Ag. In this device, TiO2 act as ETM, CsPbBr3 act as active perovskite layer and NiO plays the role of HTM.

The I-V characteristics of solar cell device can be measured using solar simulator setup. The dark current and photo current response of the solar cell can be obtained. The input of the solar simulator is 1000W/m^2 (Standard AM 1.5 spectrum). When this light falls on the device, the I-V characteristics are obtained.

3.2 Characterization Techniques:

3.2.1 X-Ray Diffraction

X-rays are electromagnetic waves, discovered by German physicist in 1895 [**20**] and were named so because at that time their characteristics were not known. Although, its use was started in radiography as it was known that X-rays can penetrate opaque objects and hence its use in medical science was done for the imaging of different body parts for fracture determination. In 1912, X-ray diffraction phenomenon by crystals was identified and simultaneously its wave nature was identified. This states that if crystals were made up of regularly spaced atoms and acts as scattering centres for X rays and if X rays are electromagnetic waves then by using crystals it

should be possible to diffract X rays [**21**]. This provided a new methodology for the investigation of structure of the crystals.

X-ray diffraction is a tool for investigating the crystal structure of the material. It is observed that X-rays gets diffracted when passed through the crystals and the angle of diffraction provides information about its structure. Diffraction can indirectly bring up the details regarding the internal structure of the order of 10^{-8} cm in size .Earlier X ray diffraction was used to determine the crystal structure of any substance but later on it was applied for the purpose of stress measurement, for calculation of particle size, to study phase equilibrium, chemical analysis and also for determining the orientation of single crystals or the assembly of different crystals in a polycrystalline material.

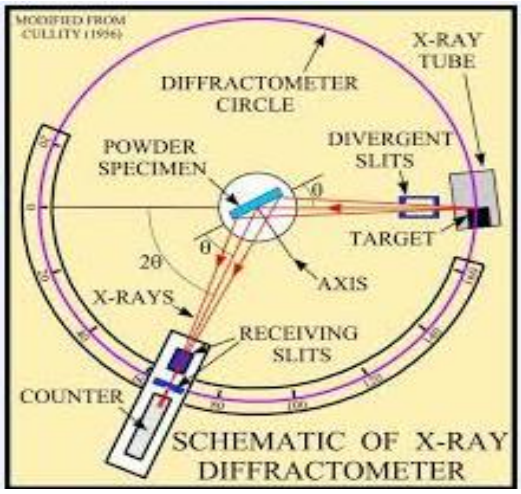

Fig. 7 Diffraction spectrometer [22]

Brags Law

Brags law is special case of Laue diffraction, which gives the angles of coherent and incoherent scattering from a crystal lattice [**23**]. The peaks of

scattered X-rays from the crystal lattice are observed to determine its crystal structure. This refers to the following conditions:

(i) Angle of incidence = Angle of scattering

(ii) The path difference is equal to integral multiple of wavelength

i.e. $\mathbf{n\lambda = 2d \sin\Theta}$

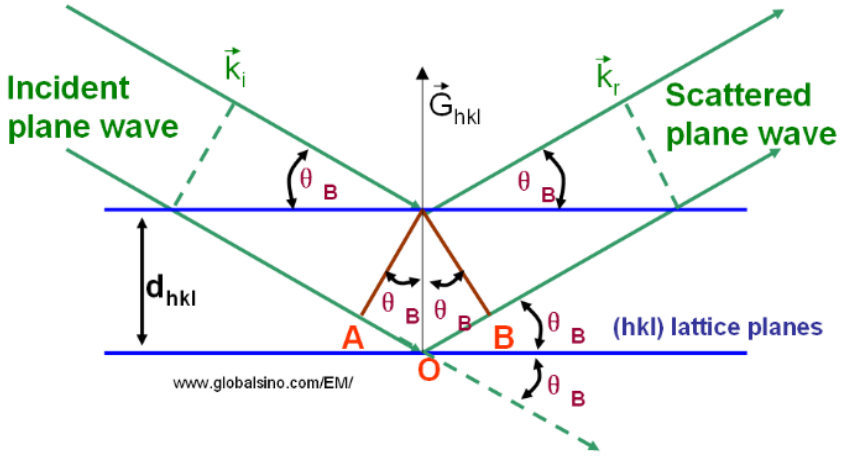

Fig. 8 Braggs law [24]

Two grometrical facts are worth remembering :

- The incident beam, deffracted beam and the normal to the reflectig plane always lie in the same plane.
- The angle between diffracted beam and transmitted beam is always 2Θ, and it is known as diffraction angle. This is the angle which is measured while all experimental studies instead of angle Θ.

3.2.2 UV Visible spectroscopy

Ultraviolet visible spectroscopy or UV-Visible spectroscopy refers to the absorbance, reflanctance and transmitance spectroscopy that in the ultra violet and visible region of the spectrum from 200nm to 800nm. particularly, UV region lies in the spectral wavelength of 200-400nm while visible region belongs to 400-800nm of the spectrum. Absorbance of ultraviolet or visible light is related with the excitation of electron from lower energy states to higher energy states. When a sample is kept inside the UV spectrometer, it absorbs the light energy when it is sufficient to produce the excitation of electron present within the molicule or atom of the specimen. The wavelength at which maximum absorbance occurs is known as λ_{max} and is known as intensity of maximum absorbance and is denoted by ϵ_{max}.

Fig. 9 UV visible spectrometer [25]

UV Visible spectrometer is used to calculate the absorbance of ultra violet and visible light by a sample. It can be performed at a particular value of wavelength or at different wavelengths available in the spectrum. The technique can be used both qualitaively and quantitatively. The light source is a combination of tungsten/ halogen and deuterium lamps that emits the light energy ranging from 200-800nm. The output of the source falls on the diffraction grating that splits the light into components of colours at

different wavelengths. After that, the light falls on the beam splitter, where it distributes in two sections and passes through the sample (under testing) and the reference. For each wavelength the intensity of light passed hrough sample(I) and the reference (I_0) is measured. The absorbance of sample is dependent on the values of I and I_0 and is given as :

$$\mathbf{A = \log (I/I_0)}$$

Beer-lambert law

Acording to Beer lambert law, the absorption of solution is propotional to the concentration of the substance and also to the optical path length i.e. the dimention of the cuvette. Mathamatically,

$$A \propto \mathbf{c.l}$$

$$\mathbf{A} = Є.\mathbf{c.l}$$

Where,

C is the concentration of the substance in mol dm^{-1}

L is the optical length in cm, and

Є is the propotionality constant also kniwn as molar extenction (dm^3 $mol^{-1}cm^{-1}$)

Note: The UV Visible spectra of TiO_2 thin film shows the maximum absorbance in the ultravoilet range of the spectrum, while behaves transparent for the visible light. High transmittance of the film is desired in our application and therefore the thin film is optimised by doing variation in time and temprature.

3.2.3 Field Emission Scanning Electron Microscope (FESEM)

Field emission scanning electron microscope is an electron microscope as it uses electrons instead of light to produce the image of the sample. The FESEM can observe structures upto 1nm (billionth of a millimeter). The electrons are made to strike the surface of the sample that results in absorbtion or reflection of these electrons at the sample surface. Also, these striking electron might take out an electron form the sample material md that is termed as secondary electron. The diferent types of electrons obtained tells about the details of surface morphology of the specimen. Different detectors are mounted to detect the electrons comming from the sample and hence to determine the surface morphology. Backscattered electrons tells about the percentage composition of the sample while secondary electron tells about the surface topology of it.

Fig. 10 FESEM Setup

The electrons are liberated from a field emission source and are accelerated at high velocities in electric field gradient. These primary electrons are focussed in a vacuum column and deflected by electronic lenses to obtain narrow scan beam of electrons that strikes on the Specimen for the image formation. The angle and velocity of secondary electrons produced gives the information about the surface topology of the sample.

Proper sample preparation plays vital role in observing its SEM images as the sample which is under observation should be conductive. Generally, FTO is used as the substrate to ensure the conductivity of the prepared thin film but in many cases where glass substrate is used, gold sputtering is done to make the sample conductive in nature.

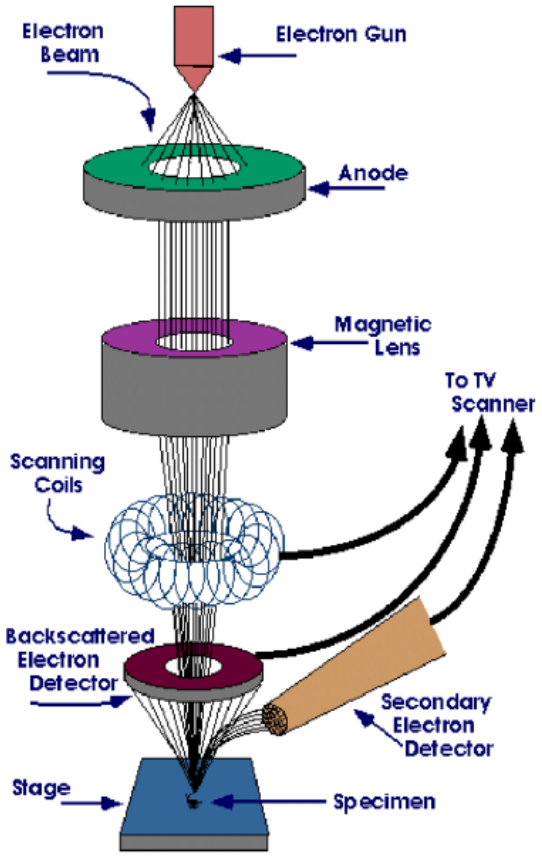

Fig. 11 Schematic of FESEM [26]

The fig. shows the schematic of FESEM machine that comprises of an electron gun that generates the electrons which are then directed towards condenser lens that acts as anode and due to its positive charge, it controls the size of beam and amount of electron going down the column. After passing through condenser lens, the electron beam enters observer lens and focuses the beam at a spot on the sample. When the electron strikes the specimen/sample, it results in the generation of backscattered electrons, secondary electrons, auger electrons, X-rays, etc. The surface morphology is obtained by observing the deflection and the velocity of the new generated electrons.

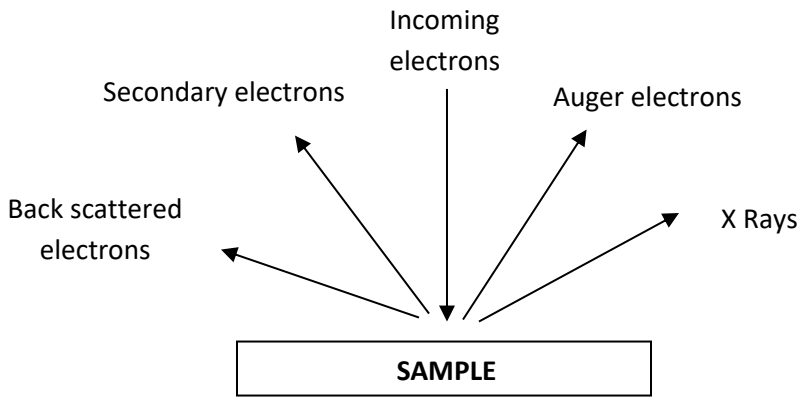

Fig. 12 Emission of different electron signals from the specimen placed inside FESEM

3.2.4 Electrochemical Setup Measurements:

The image shown below is the three-electrode electrochemical setup that can be used for different techniques like chronoamperometry, cyclic Voltammetry, open circuit potentiometry etc. Here, the red colour electrode is the working electrode, while the blue and green black colour electrodes are reference and counter electrodes. The green coloured electrode is

connected to ground for safety of the instrument in over current and over voltage conditions.

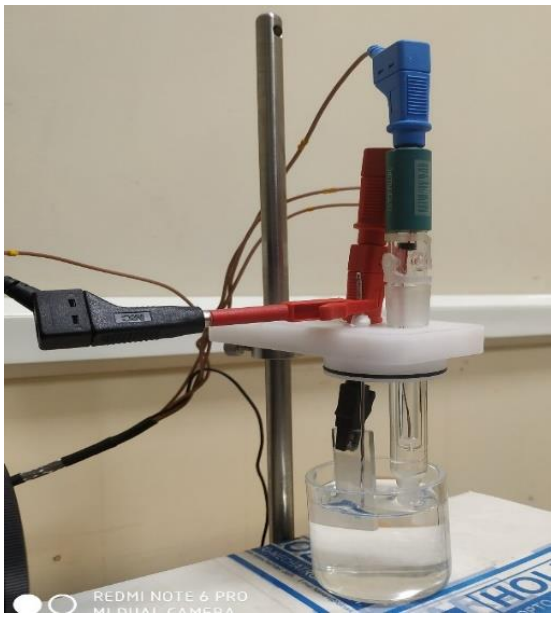

Fig. 13 Three-electrode electrochemical setup

(a) Chronoamperometry:

Chronoamperometry is an electrochemical technique used to monitor the kinetics of a chemical reaction. In this technique, the variation of current versus time is monitored with or without application of a step voltage. The setup for chronoamperometry consists of three electrodes including working electrode, counter electrode and reference electrode. The reference electrode is the Ag/AgCl electrode while the counter electrode is made of platinum. TiO_2 thin film was prepared to act as the working electrode and the current was measured for sample prepared at different conditions.

(b) Cyclic Voltammetry:

Cyclic Voltammetry is a potentiodynamic electrochemical technique in which the applied voltage is swept between two voltage levels (say V_1 and V_2) at a fix rate. However, when the voltage reaches V_2 the scan is reversed, and the voltage is swept back to V_1.

The forward scan produces an identical response to that of LSV experiment, but when the scan is reversed, the process simply reversed, and equilibrium products are simply converted back into the reactants. The CV scans of any thin film can determine its stability. If the cyclic voltammogram of thin films follows the same path in multiple paths, then it is supposed to give stable performance.

(c) Open Circuit Potentiometry:

Open circuit potentiometry is also an electrochemical technique which is done on the similar three electrode setup used for chronoamperometry and cyclic Voltammetry. During this process, there is no current flowing in the working electrode as the connection is open circuited. Using this technique, we can measure career life time of charge careers in the semiconducting materials. The open circuit voltage decay is a conventional method for calculating the career lifetime. When the light source is removed, the stored charge careers recombine and decay exponentially. The decay curve is Gaussian fitted and then the slope value of voltage with respect to time is determined to calculate the career life time using the formula given bellow **[27]**:

$$\tau = -\frac{K_b T}{e}\left(\frac{\mathrm{dVoc}}{\mathrm{dt}}\right)^{-1}$$

CHAPTER 4

RESULTS AND DISCUSSIONS

At the beginning, the variation in size and shape of TiO_2 nanostructure with respect to time will be discussed. After complete analysis and optimization of this parameter, we will also study the variation in the nanostructure with change in precursor concentration.

4.1 Effect of Variation in Time on TiO_2 Nanostructures:

4.1.1 Structural Study of TiO_2 Nanostructures:

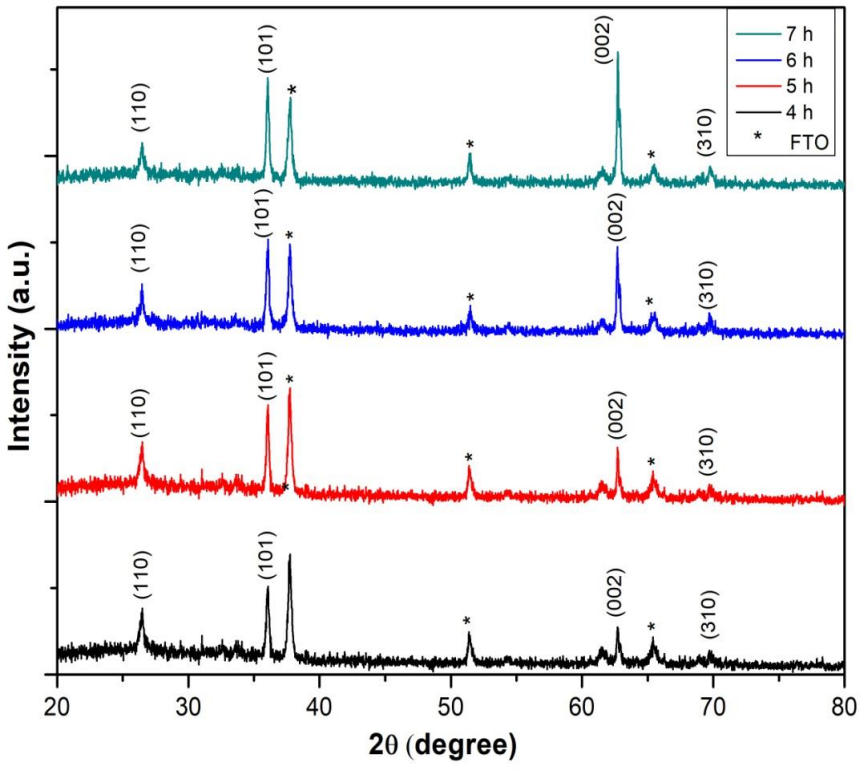

Fig. 14: XRD pattern of TiO_2 nanostructure samples prepared at different reaction times

The crystallite size and crystal structure of TiO_2 thin films was confirmed from the XRD analysis **[28]**. Figure shows XRD pattern of different TiO_2 thin films prepared at varying reaction times. XRD pattern shows high intensity diffraction peaks at 27.55°, 36.8°, 62.85° and 69°, which indicates the formation of rutile phase TiO_2. The diffraction peaks at 27.55° and 62.85°are the representative peaks of rutile phase and the other strong peaks confirm the tetragonal crystal structure of TiO_2. Amongst (110) and (002) peaks, the intensity of (002) peak is majorly affected by varying reaction time. This shows that, growth of rutile phase TiO_2 is highly oriented in (002) plane of FTO substrate during hydrothermal reaction. The formed nanostructures are in single crystalline form. All peaks are in perfect order and the obtained result was confirmed using ICSD card no- 98-001-2307.

Crystallite size of the TiO_2 nanorods can be determined using the relation: **[29]**

$$D = \frac{0.9\lambda}{\beta cos\Theta}$$

where,

D is the crystallite size

λ is the wavelength of the x ray

β is full width half maxima (FWHM)

Θ is the diffraction peak position

4.1.2 Optical Properties of TiO_2 Nanostructure by UV-Visible Spectroscopy:

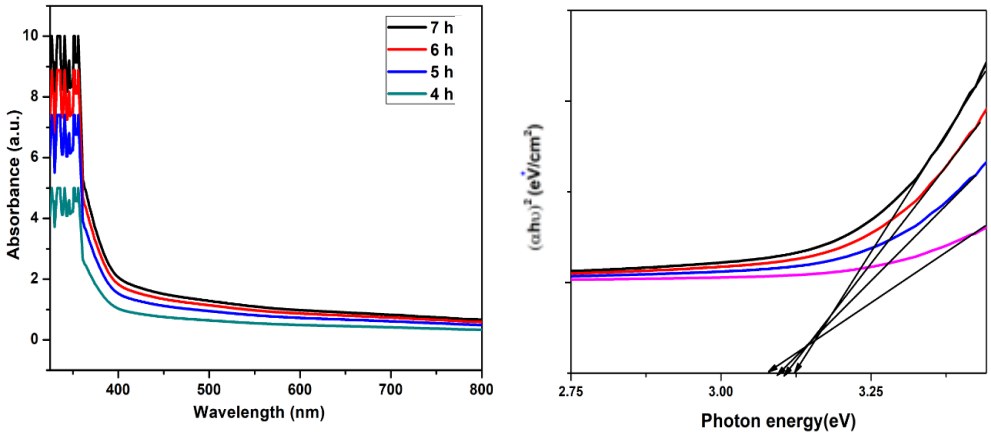

Fig. 15 (a) UV Visible absorption spectra of TiO_2 thin films hydrothermally grown for different reaction times. (b) Tauc plot of $(\alpha h\nu)^2$ vs $h\nu$ of TiO_2 thin films.

The optical properties were observed by the absorption spectra of the thin films prepared hydrothermally at 160°C for different reaction times (4 to 7 hours). The fundamental of absorption is related with the excitation of electron from lower energy states to higher energy states. The absorption coefficient (α) as function of photon energy can be expressed using Tauc relation **[30]**:

$$\alpha h\nu = \alpha(h\nu - E_g)^n$$

where,

α is absorption constant

$h\nu$ is photon energy

E_g is energy band gap

n is the exponential index and its value is determined by type of electron transition i.e. for direct band gap material (n=1/2) and for indirect band gap (n=2). Using Tauc relation, the band gap for our material is found out to be 3.1 eV.

4.1.3 FESEM Images:

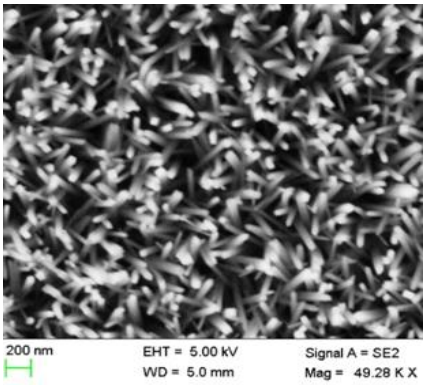

Reaction time 4 hrs
Precursor concentration 0.7 ml
Temperature 160^0C

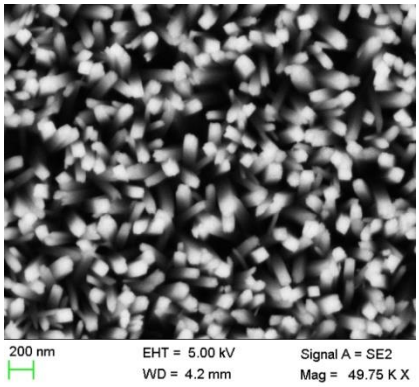

Reaction time 5 hrs
Precursor concentration 0.7 ml
Temperature 160^0C

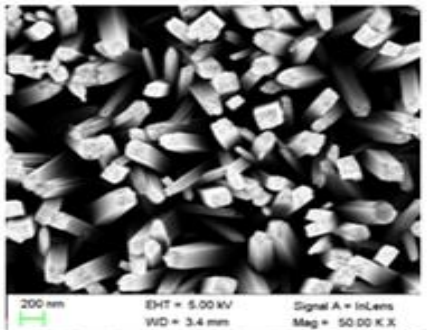

Reaction time 6 hrs
Precursor concentration 0.7 ml
Temperature 160^0C

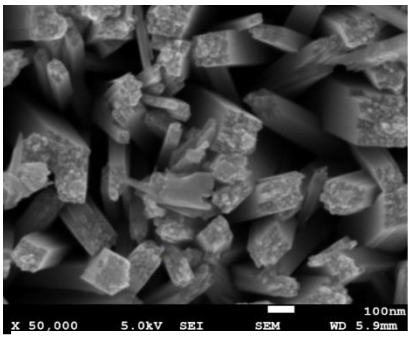

Reaction time 7 hrs
Precursor concentration 0.7 ml
Temperature 160^0C

Fig. 16 FESEM Images of TiO_2 Nanorods at different reaction times

The FESEM images show that the size, shape, orientation and morphology of the Nanorods are mainly dependent on reaction time. At less reaction time, the Nanorods are uniformly grown and compact because of immature

termination of growth process and shows good photo electrochemical properties. As the reaction time is increased, impulsive aggregated Nanorods are obtained which shows lower photo electrochemical performance due to its compactly arranged structure. With increase in reaction time, it can clearly be observed that the

4.1.4 Photocurrent Measurement:

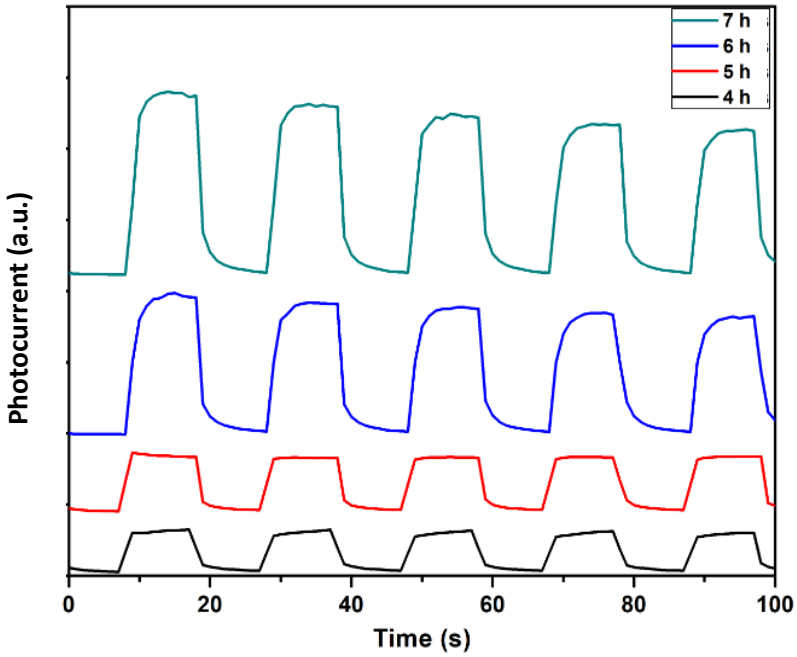

Fig. 17 Photocurrent response of TiO_2 thin films

All TiO_2 thin films prepared at different conditions shows excellent photocurrent response and shows stable output after multiple cycles. Although, the intensity of photocurrent is maximum in the case of sample prepared for 7 hrs but since we are getting stable photo response with better transparency in the TiO_2 sample prepared for 4 hrs, this is the most optimised result for perovskite solar cell application.

4.1.5 Cyclic Voltammetry:

Cyclic Voltammetry is a potentiodynamic electrochemical technique in which the applied voltage is swept between two voltage levels (say V_1 and V_2) at a fix rate. However, when the voltage reaches V_2 the scan is reversed, and the voltage is swept back to V_1.

0The forward scan produces an identical response to that of LSV experiment, but when the scan is reversed, the process simply reversed, and equilibrium products are simply converted back into the reactants. The CV scans of any thin film can determine its stability. If the cyclic voltammogram of thin films follows the same path in multiple paths, then it is supposed to give stable performance.

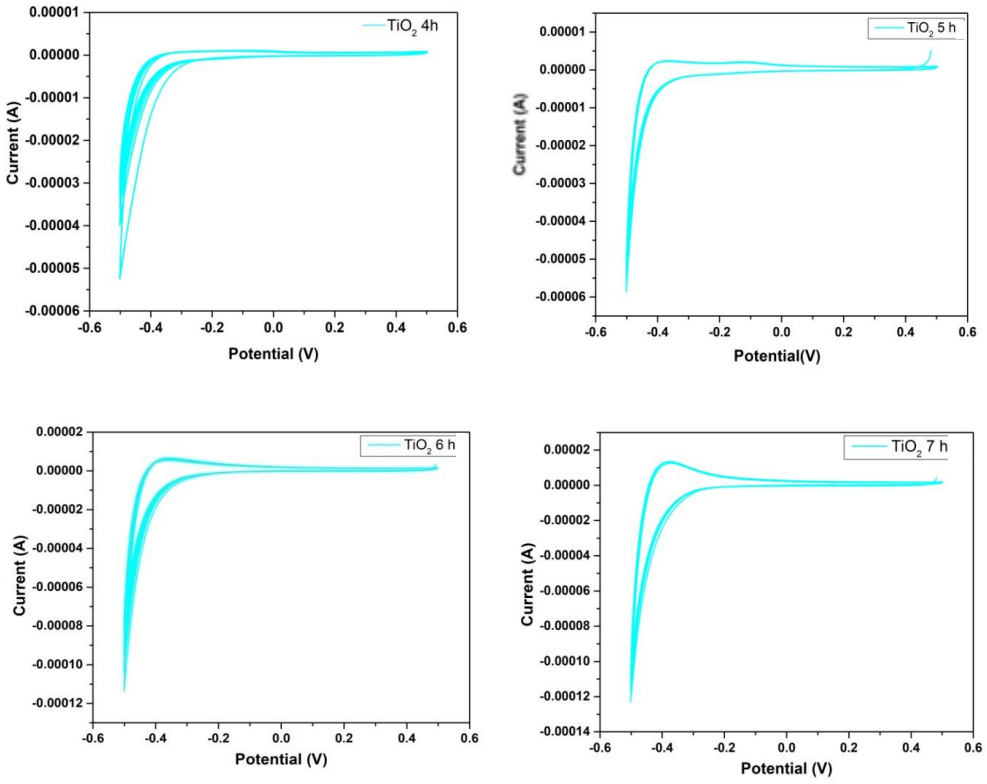

Fig. 18 Cyclic Voltammetry for TiO_2 samples at scan rate of 10 mV/sec prepared at different reaction times

4.1.6 Open Circuit Potentiometry:

The open circuit potentiometry is an electrochemical technique under zero current conditions. This technique has many important applications including the calculation of career life time in any semiconducting material. In our case, we are performing this experiment to calculate the career life time of the charge carriers in TiO_2 thin films. During the experiment, when the light source is removed from the sample, the recombination of charge careers takes place and there is decay in the open circuit voltage (V_{oc}), which is used for the measurement of life time of charge careers in the material.

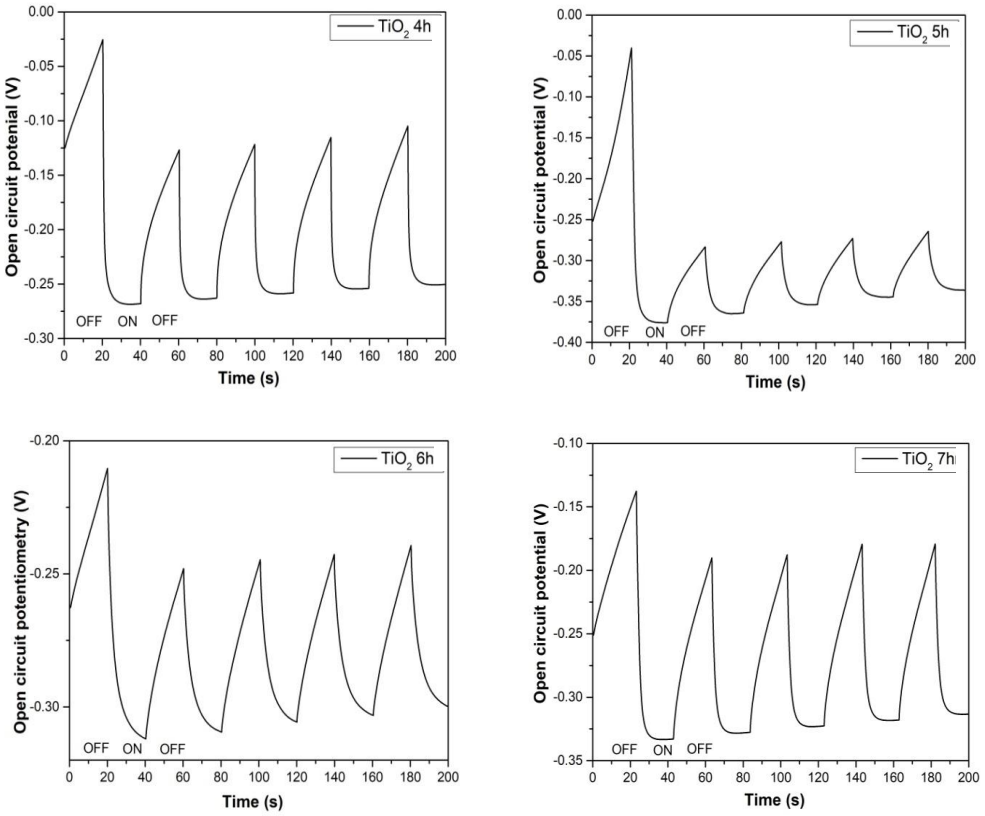

Fig. 19 Open circuit potentiometry of TiO_2 thin films at different reaction times

The charge carrier's recombination time with respect to V_{oc} in TiO_2 thin films can be calculated using the given relation:

$$\tau = -\frac{K_b T}{e}\left(\frac{\mathrm{dVoc}}{\mathrm{dt}}\right)^{-1}$$

To determine the carrier life time of electrons and holes in the TiO_2 thin films, the value of $\frac{dV_{oc}}{dt}$ is to be calculated. To obtain this rate of change of slope with respect to time, Gaussian fitting of the curve is required. After obtaining the value of this factor, we can determine the value of carrier life time in our samples. We will calculate the carrier life time for the both extremities i.e. for sample with parameters 0.7 ml concentration and 4 h reaction time and for sample having 0.7 ml concentration and 7 h reaction time to obtain the trend of life time of the charge carriers.

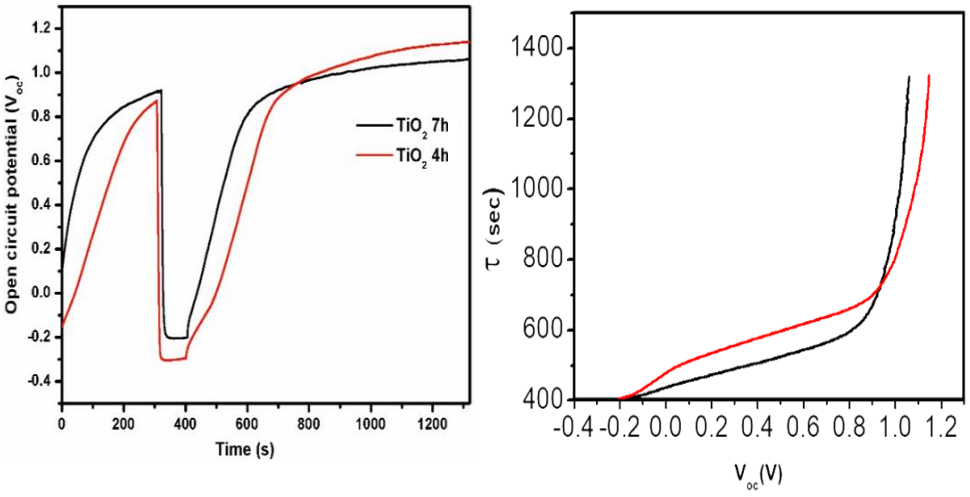

Fig. 20 OCV for TiO_2 samples with reaction time 4 h and 7 h

The TiO_2 thin film prepared in 4 h shows higher carrier lifetime than the thin film prepared in 7 h. This is because of the impulsive aggregation of nanorods that lower the photoelectrochemical performance due to its compactly aggregated structure.

4.2 Effect of Variation in Precursor Concentration on TiO_2 Nanostructures:

The change in precursor concentration results change in nucleation density and growth rate of TiO_2 Nanorods. Hence, the density, morphology and aspect ratio of these nanostructures are directly affected by the change in concentration of Titanium butoxide. We prepared are TiO_2 samples for different concentrations of 0.5 ml, 0.7 ml and 0.9 ml respectively. At low concentrations, poor alignment of TiO_2 Nanorods was observed. Also, the diameter and the length of Nanorods was minimum in case of low precursor concentration. As the concentration of Titanium butoxide was increased, more aligned nanostructures were obtained with larger aspect ratios. Although, the increase in the length of the Nanorods were not following a continuous trend. We can say that the increase in length after a while is not very significant.

4.2.1 Structural Analysis of TiO_2 Nanostructures:

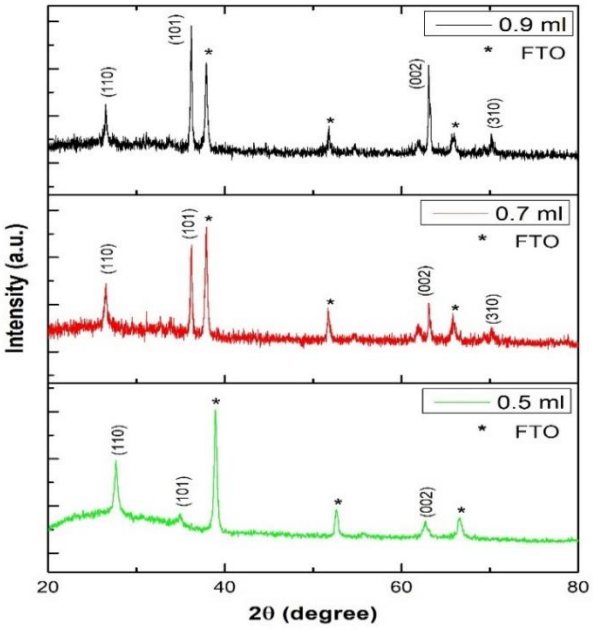

Fig. 21 XRD pattern of TiO_2 nanostructures prepared at different precursor concentration

With variation in precursor concentration, the intensity variation in different peaks are observed. The intensity of (101), (002) and (310) phases increase with increase in the precursor concentration while the (110) peak intensity is observed to be slightly reduced. We can observe the changes in the intensity of phases in the XRD pattern shown in the Fig. 23

4.2.2 Study of optical properties of TiO_2 nanostructures with change in precursor concentration:

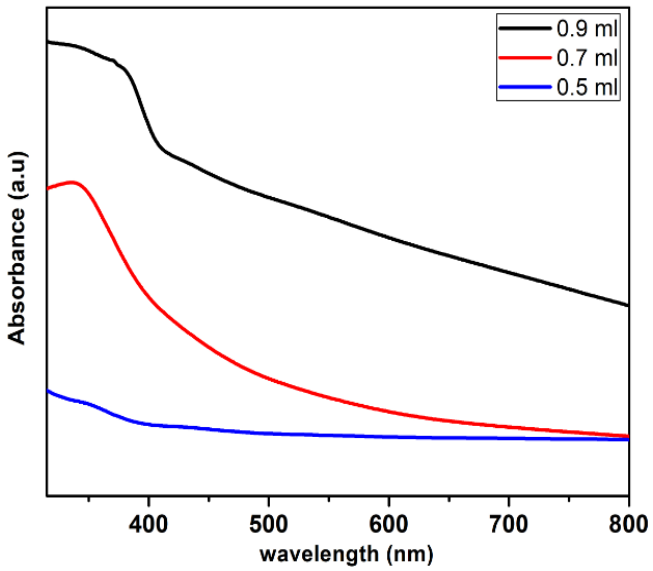

Fig. 22 UV Visible of TiO_2 samples prepared at different precursor concentrations

Fig shows the UV Visible spectroscopy results for different concentration of Titanium butoxide i.e. 0.5 ml, 0.7 ml and 0.9 ml respectively. The maximum absorption is again obtained in the UV range around 325 nm range in spectrum. In visible region, the maximum transparency is obtained in the sample prepared with minimum concentration but as the alignment of Nanorods in this case is not proper, the desired photocurrent properties cannot be obtained. In TiO_2 sample with highest concentration i.e. 0.9 ml, the photocurrent response is expected to be the best, but it lacks in transparent nature in visible range. Hence the TiO_2 sample prepared at 0.7

ml of Titanium butoxide for 4 hours is the most optimised thin film when it comes to parameters like transparency, electrical conductivity and career lifetime.

4.2.3 FESEM Images:

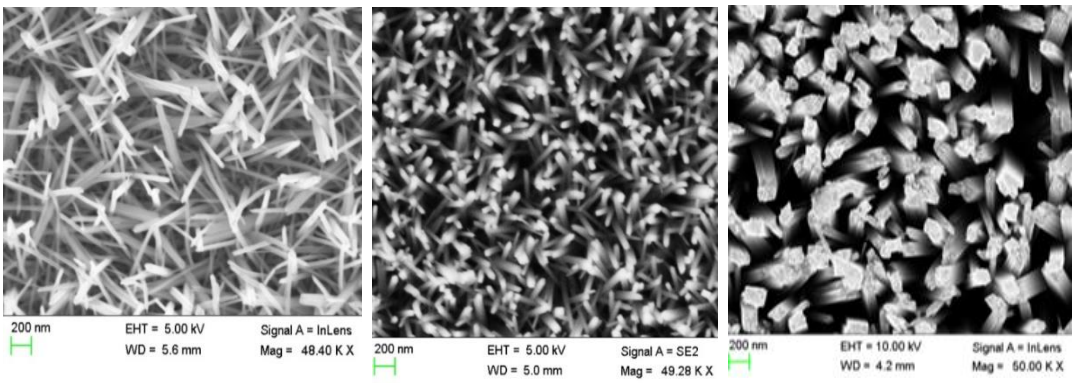

Reaction time 4 h
Precursor concentration 0.5ml
Temperature 160^0C

Reaction time 4 h
Precursor concentration0.7ml
Temperature 160^0C

Reaction time 4 h
Precursor concentration 0.9ml
Temperature 160^0C

Fig. 23 FESEM Images of TiO_2 Nanorods at different precursor concentration

The growth and nucleation density of TiO_2 nanorods are dependent upon precursor concentration. The density, morphology and aspect ratio of the nanostructures varies with change in the precursor concentration. We prepared TiO_2 thin films at different concentrations of titanium butoxide and it was observed that the samples prepared at low concentration were having lower length and diameter of nanorods. Also, the nucleation density was less for the thin films with less precursor concentrations. The nanorod were not properly aligned and they continue to grow at certain angles. As the concentration was increased, the nanorods became more longer and thicker as compared to the ones at lower precursor concentrations. On the other hand, the growth was much denser because of more nucleation sites present due to more concentration of precursor taken. At high concentration, the nanorods growing at an angle to the substrate surface, run into

neighbouring nanorods and stop growing. i.e. the growth in length is restricted but proper alignment is obtained **[31]**. As we can see in the Fig. 25, the TiO_2 thin films prepared at 0.5 ml concentration has less diameter and nucleation density. The sample with 0.9 ml precursor concentration has very thick rods with very high density of nanorods. The thin films at 0.7 ml concentration thin film shows the optimum aspect ratio of the nanorods. The thin film obtained was transparent and shows good photocurrent response and hence can be considered as the optimised sample for usage as electron transport layer in perovskite solar cell fabrication.

4.3 $CsPbBr_3$ Perovskite Nanoparticles:

4.3.1 Structural study of Perovskite Nanoparticles:

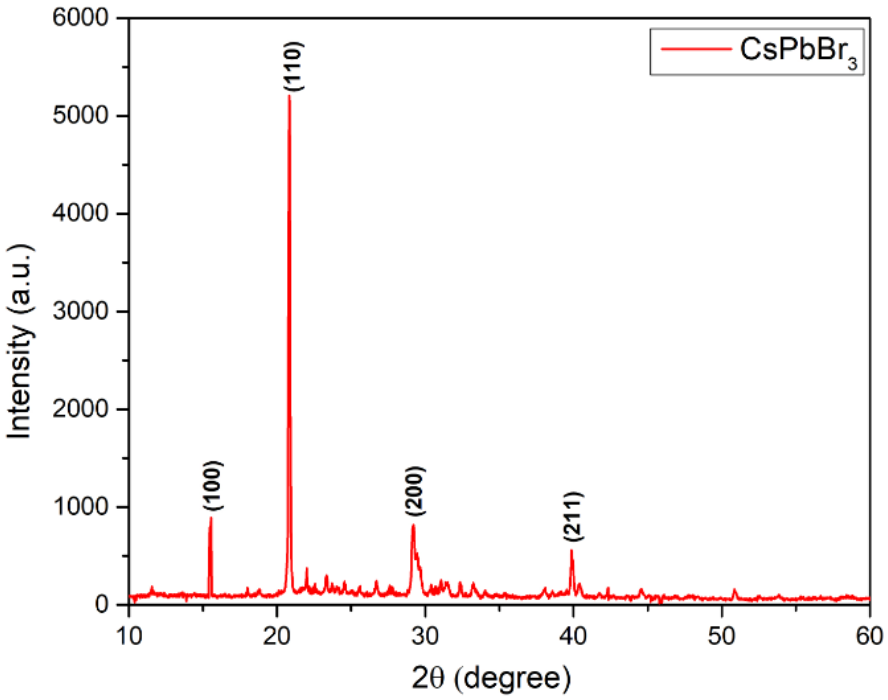

Fig. 24 XRD pattern of $CsPbBr_3$

The X-Ray diffraction measurements of the perovskite thin films was performed, and the analysis confirms the structural formation of $CsPbBr_3$

perovskite material. The scan was done at the rate of 5° per minute with step size of 0.01°. The high intensity diffraction peaks are observed at 15.55°, 21.20°, 29.45° and 39.94° for (100), (110), (200) and (211) planes respectively **[32]**. Major growth of perovskite structure is highly oriented along (110) plane of the FTO substrate. The obtained spectra were compared with the ICSD file 98-000-5868 and the structural growth was confirmed.

Impurity peaks were observed in case of the perovskite that was prepared with 1:1 molar ratio of the precursors. These impurities might be present due to equal molar ratio of Cs^{+2} and Pb^{+2} taken which leads to the formation of $CsPb_2Br_5$. This impurity can be removed by taking different molar ratio of precursors.

4.3.2 Optical Behaviour of Perovskite Nanoparticles:

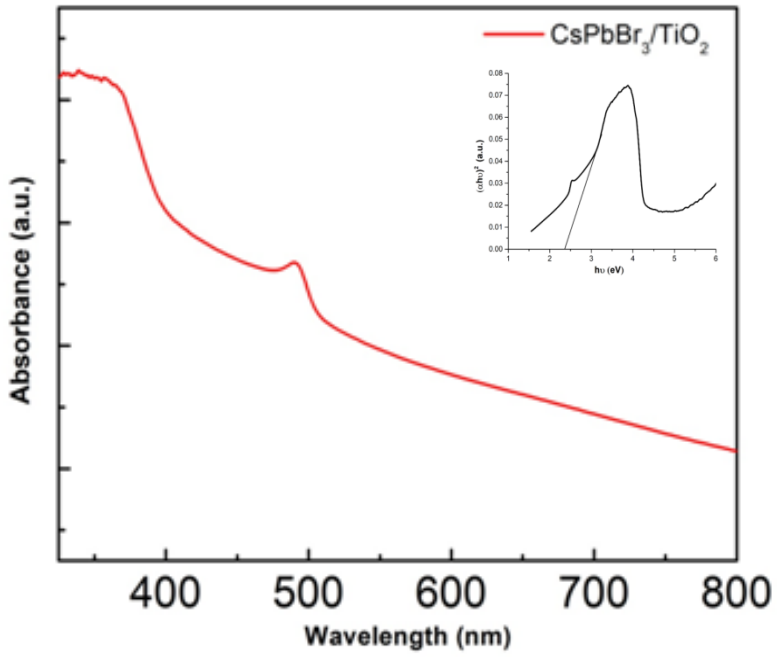

Fig 25. UV Visible absorption spectra of $CsPbBr_3$

The absorption spectrum of $CsPbBr_3$ is obtained and a sudden bump around 510 nm was observed where the maximum absorbance of perovskite was

observed. The band gap of the material was calculated using the Tauc relation. As $CsPbBr_3$ behaves as direct bandgap material, the tauc plot is plotted between $(\acute{\alpha}h\nu)^2$ and $h\nu$. By extrapolation the curve, the bandgap was found out to be 2.3 eV. **[33]**

4.3.3 FESEM Images:

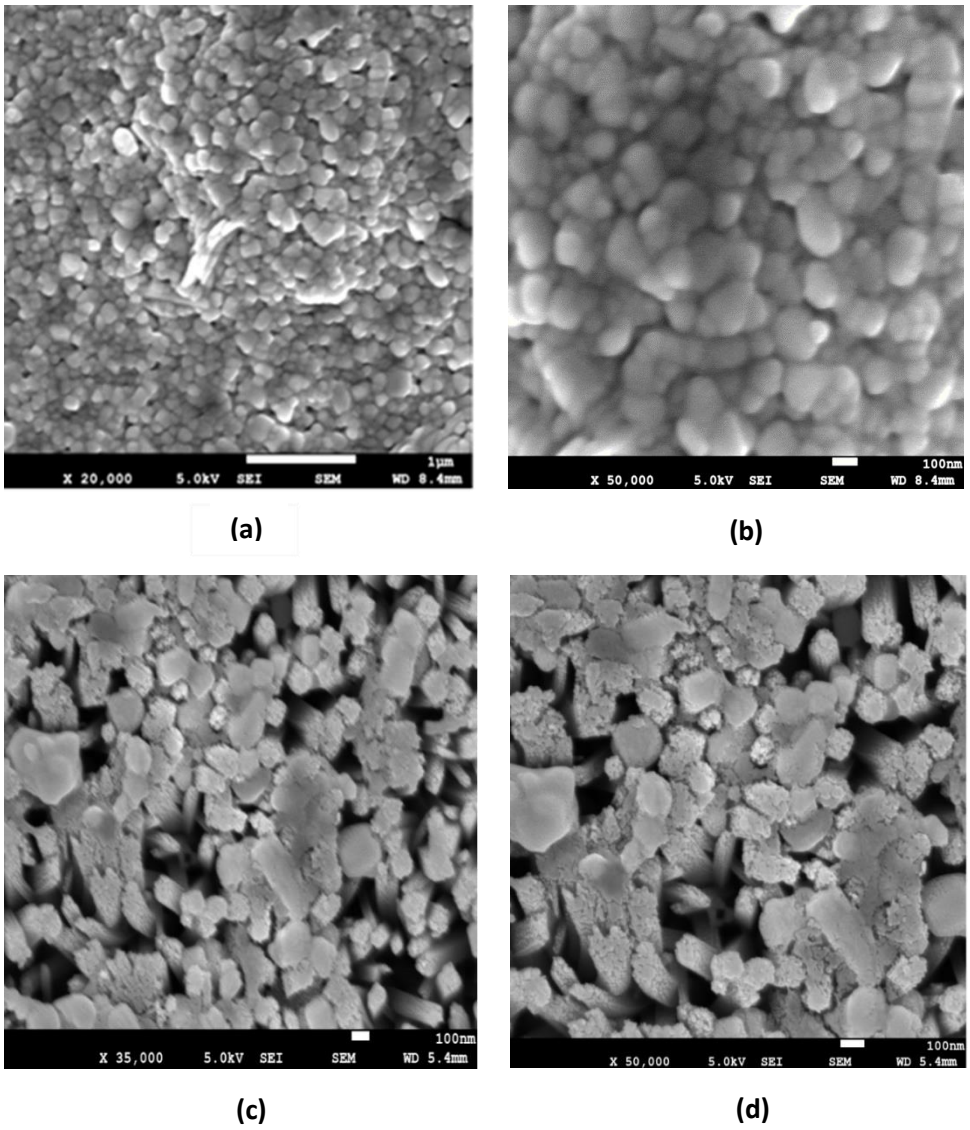

Fig. 26 (a) and (b) shows FESEM Images of Inorganic perovskite $CsPbBr_3$, while (c) and (d) shows $CsPbBr_3$ coated over TiO_2 nanorods

The FESEM images of Perovskite nanoparticles deposited over FTO substrate shows its uniform growth and morphology. After successful deposition of perovskite material on bare FTO, we tried to coat it over the TiO_2 nanorods so as to confirm if their structure matches while intermixing. The images (c) and (d) shows the FESEM images of perovskite coated over the TiO2 nanorods at different magnifications. It is observed that the perovskite particles get inside the voids available around the TiO_2 nanorods which is necessary for proper mixing of both layers.

4.4 Fabrication of FTO/ TiO_2 / $CsPbBr_3$ / NiO /Ag:

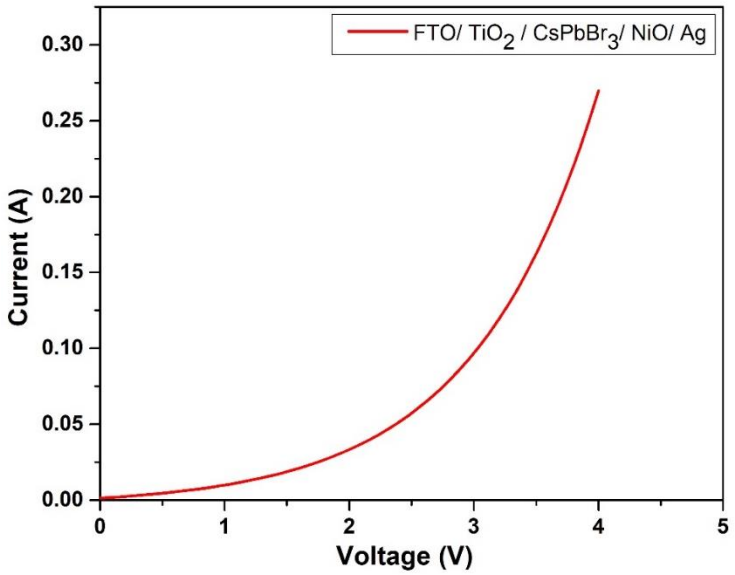

Fig. 27 Dark Current profile for FTO/ TiO_2 / $CsPbBr_3$ / NiO /Ag

The approach towards device fabrication resulted in the IV characteristics of FTO/ TiO_2 / $CsPbBr_3$ / NiO /Ag. The fabrication involved the growth of TiO_2 nanorods over FTO substrate, followed by deposition of $CsPbBr_3$ layer over it. The NiO nanoparticles were spin coated over it to develop the p-region of the device. The curve obtained resembles the p-n junction diode characteristics. The result is obtained is termed as the dark current profile of our device. However, our device did not show any photo response in presence of light.

CHAPTER 5

CONCLUSION AND FUTURE OUTLOOK

In this work, we prepared TiO_2 based electron transport material for the application in perovskite solar cell. The preparation of TiO_2 NR's was done by facile hydrothermal synthesis in which we took Titanium butoxide as the reaction precursor. The synthesis was done at different reaction times and precursor concentrations in order to optimise our samples in terms of conductivity, stability, photo-response and transparency. The sample that was prepared with 0.7ml of Titanium butoxide for 4 hours of reaction time at 160 degree, showed the best performance in all aspects including optical properties, photocurrent response and long-term photo stability. We also synthesised the inorganic perovskite material $CsPbBr_3$ by solution processing method. Its structure was confirmed by the XRD analysis and the bandgap was found out to be 2.3 eV. The SEM images showed the uniformly distributed particles all over the FTO surface. We tried to intermix both the layers i.e. ETL and active perovskite layer to get one step closer in the preparation of the perovskite solar cell.

In future, a lot of work can be done in order to get highly efficient device with good PCE. The performance in active perovskite layer can be done by addition of some impurities like changing the halide group or making changes the alkali metal. The complete or partial replacement of these groups might result in increased power conversion efficiency and also their ambient stability. By preparation of hole transport layer using inorganic materials like NiO, carbon etc. we can get the all the required layers for the operation of the a stable all inorganic solar cell device.

REFERENCES

1)Nozick, A.J. (2002)" Quantum dot solar cells." *Physica E: Low-dimensional Systems and Nanostructures* 14.1-2: 115-120.

2) Squirmymcphee, 19 October 2008

3) NREL, www.nrel.gov/ncpv 2016

4) Sharma Shruti, Kamlesh Kumar Jain, and Ashutosh Sharma. (2015) "Solar cells: in research and applications—a review." *Materials Sciences and Applications* 6.12: 1145.

5)Goetz Berger, Adolf, Joachim Knobloch, and Bernhard Voss. (1998) "Crystalline silicon solar cells." *editorial John Wiley & Sons Ltd*1.

6) Lacerda, Juliana Subtil, and Jeroen CJM van den Bergh. (2016) "Diversity in solar photovoltaic energy: Implications for innovation and policy." *Renewable and Sustainable Energy Reviews* 54: 331-340.

7) Moreira, Mario L., et al. (2009) "Structural and optical properties of $CaTiO_3$ perovskite-based materials obtained by microwave-assisted hydrothermal synthesis: An experimental and theoretical insight." *Acta Materialia* 57.17: 5174-5185.

8) X. Li, D. Bi, C. Yi, J. D. Decoppet, J. Luo, S. M. Zakeeruddin, A. Hagfeldt, M. Gratzel, (2016) Science, 353, 58

9) Y. Hu, F. Bai, X. Liu, Q. Ji, X. Miao, T. Qiu, S. Zhang, (2017) ACS Energy Lett., 2, 2219

10) W. S. Yang et al (2017) Science, 356,1376

11) Jung, Hyun Suk, and Nam-Gyu Park. (2015) "Perovskite solar cells: from materials to devices." *small* 11.1: 10-25

12) Zhou, Huanping, et al. (2014) "Interface engineering of highly efficient perovskite solar cells." *Science* 345.6196: 542-546.

13) Kong, Fan-Tai, Song-Yuan Dai, and Kong-Jia Wang. (2007) "Review of recent progress in dye-sensitized solar cells." *Advances in Optoelectronics* 2007.

14) Kim, Hui-Seon, et al. (2013) "High efficiency solid-state sensitized solar cell-based on submicrometer rutile TiO_2 nanorod and $CH_3NH_3PbI_3$ perovskite sensitizer." *Nano letters* 13.6: 2412-2417.

15) Shinde, D. B., et al. (2015) "Time dependent facile hydrothermal synthesis of TiO_2 nanorods and their photoelectrochemical applications." *J Nanomedic Nanotechnol S* 7: 2.

16) Mo, Shang-Di, and W. Y. Ching. (1995) "Electronic and optical properties of three phases of titanium dioxide: Rutile, anatase, and brookite." *Physical Review B* 51.19: 13023.

17) AIST: https://unit.aist.go.jp/rcpv/cie/r_teams/eFTFT/index.html

18) Liu, Bin, and Eray S. Aydil. (2009) "Growth of oriented single-crystalline rutile TiO2 nanorods on transparent conducting substrates for dye-sensitized solar cells." *Journal of the American Chemical Society* 131.11: 3985-3990.

19) Joshi, Mangala, A. Bhattacharyya, and S. Wazed Ali. (2008) "Characterization techniques for nanotechnology applications in textiles.".

20) B D Cullity, (1956) Elements of X-ray Diffraction.

21) E. N. Maslen, A. G. Fox, M. A. O'Keefe, (2004) X-ray Scattering, in: E. Prince (Ed), International Tables for Crystallography, Vol. C (Kluwer Academic, Dordrecht, p. 554.

22) Seely, John, et al. (2014) "Measurement of the O2O3O4 and O3O4O5 super Coster–Kronig rates in tungsten via asymmetric diffraction spectrometry." *Journal of Physics B: Atomic, Molecular and Optical Physics* 47.11: 115004.

23) Jauncey, G. E. M. (1924) "The scattering of x-rays and Bragg's law." *Proceedings of the National Academy of Sciences of the United States of America* 10.2: 57.

24) Tanner, (1976) Brian Keith. *X-ray diffraction topography*. Vol. 84. Oxford: Pergamon press.

25) http://people.iiti.ac.in/~sic/index.php?q=uv, SIC IIT Indore

26) Joshi, Mangala, A. Bhattacharyya, and S. Wazed Ali. (2008) "Characterization techniques for nanotechnology applications in textiles.".

27) Kushwaha Ajay and Mohammed Aslam. (2014) "ZnS shielded ZnO nanowire photoanodes for efficient water splitting." *Electrochimica Acta* 130: 222-231.

28) Liu, Bin, and Eray S. Aydil. (2009) "Growth of oriented single-crystalline rutile TiO_2 nanorods on transparent conducting substrates for dye-sensitized solar cells." *Journal of the American Chemical Society* 131.11: 3985-3990.

29) Almquist, Catherine B., and Pratim Biswas. (2002) "Role of synthesis method and particle size of nanostructured TiO_2 on its photoactivity." *Journal of Catalysis* 212.2: 145-156.

30) Dolgonos, Alex, Thomas O. Mason, and Kenneth R. Poeppelmeier. (2016) "Direct optical band gap measurement in polycrystalline semiconductors: A critical look at the Tauc method." *Journal of solid-state chemistry* 240: 43-48.

31) Firooz, Azam Anaraki, Ali Reza Mahjoub, and Abbas Ali Khodadadi. (2008) "Preparation of SnO_2 nanoparticles and nanorods by using a hydrothermal method at low temperature." *Materials Letters* 62.12-13: 1789-1792.

32) Dirin, Dmitry N., et al. (2016) "Solution-grown $CsPbBr_3$ perovskite single crystals for photon detection." *Chemistry of Materials*28.23: 8470-8474.

33) Kulbak, Michael, David Cahen, and Gary Hodes. (2015) "How important is the organic part of lead halide perovskite photovoltaic cells? Efficient $CsPbBr_3$ cells." *The journal of physical chemistry letters* 6.13: 2452-2456.